Science & Technology Development Journal – Engineering and Technology 2024, 7(3):2402-2414

Open Access Full Text Article

Research Article

Easy and efficient patterning of elastomer dielectric toward commercialization of triboelectric nanogenerator

Van-Tien Bui[1,2], Thu Ha Le[1,2], Gia Huy Nguyen Hoang[1,2], Anh Tuan Luu[1,2], Trung Kien Pham[1,2], Tran Van Khai[1,2,*], Thi Thai Ha La[1,2,*]

ABSTRACT

Triboelectric nanogenerators (TENGs) are an emerging technology for harnessing green energy and serving as essential power supply for self-charging mobile electronics. Achieving high electrical output in a cost-effective, large-scale production is crucial for the widespread practical application and commercialization of TENG, yet it remains significantly challenging. In this study, we present an innovative, scalable, and cost-effective approach for surface patterning of dielectric elastomer materials with the aim of advancing the commercial potential of TENG. Our method involves the preparation of a durable plastic mold featuring microwell-patterned surface (*mw*-plate mold), using plastic wastes such as disposal Petri dishes and CD discs, through a one-step dip-coating process. Subsequently, the convex-microbead-patterned polydimethylsiloxane (*mb*-PDMS) replicas are created using a micromolding technique. Our results indicate the superior structural integrity of the honeycomb mold throughout multiple molding processes, attributed to the reinforcing ability of the plastic plate. Furthermore, TENG device using *mb*-PDMS exhibit a remarkable average output power density of 3.92 $mW \times m^{-2}$ with an open-circuit voltage (V_{OC}) of 185 V and a short-circuit current (I_{SC}) of 20 μA, representing a 5-fold increase over that of unstructured TENG, thereby demonstrating significantly enhanced electrification effectiveness through surface patterning. We believe that the convergence of cost-effective, scalable and efficient surface patterning of elastomer tribomaterials might enable new prospects for the commercialization of future TENGs for blue energy harvesting that requires a network of huge numbers of TENG devices.

Key words: Honeycomb, surface patterning, molding, elastomer, triboelectric nanogenerator

[1]*Faculty of Materials Technology, Ho Chi Minh City University of Technology (HCMUT), 268 Ly Thuong Kiet Street, District 10, Ho Chi Minh City, Viet Nam*

[2]*Vietnam National University Ho Chi Minh City, Linh Trung Ward, Thu Duc District, Ho Chi Minh City, Viet Nam*

Correspondence

Tran Van Khai, Faculty of Materials Technology, Ho Chi Minh City University of Technology (HCMUT), 268 Ly Thuong Kiet Street, District 10, Ho Chi Minh City, Viet Nam

Vietnam National University Ho Chi Minh City, Linh Trung Ward, Thu Duc District, Ho Chi Minh City, Viet Nam

Email: tvkhai1509@hcmut.edu.vn

Correspondence

Thi Thai Ha La, Faculty of Materials Technology, Ho Chi Minh City University of Technology (HCMUT), 268 Ly Thuong Kiet Street, District 10, Ho Chi Minh City, Viet Nam

Vietnam National University Ho Chi Minh City, Linh Trung Ward, Thu Duc District, Ho Chi Minh City, Viet Nam

Email: lathaihapolyme@hcmut.edu.vn

INTRODUCTION

The integration of healthcare sensors within the Internet of Health Things (IoHTs) demand a distributed, reliable and sustainable power source[1]. Microelectromechanical systems (MEMS technology) plays a crucial role as a driving force for reducing for shrinking the size and reducing the power consumption of these sensors[2]. Harnessing ambient energy sources, such as abundant mechanical energy readily available in the environment, present a promising solution for powering these sensors. Among the various technologies, triboelectric nanogenerators (TENGs) have emerged as exceptionally efficient in harvesting kinetic mechanical energies, such as human movements, engine vibrations, wind, flowing water, and ocean waves, into electricity[3–9]. TENGs offer numerous advantages, including flexibility, compact design, high energy-conversion efficiency, and a wide range of biomaterial choices[10,11]. While TENGs are well-known as ideal power sources for portable electronics and self-powered sensors, achieving high electrical output cost-effectively and at a large scale is imperative for their utilization in harvesting mega energy from ocean waves or wind.

Surface patterning of dielectric elastomers has been shown to significantly enhance the output performance of TENG[12]. Elastomers such as PDMS and polyurethane (PU), with specially designed surface patterns, are important functional materials in various practical applications including photonic devices[13], sensors[14], solar cells[15], soft robotics[16,17], supercapacitors[18,19], and TENG. However, conventional fabrication methods such as lithography and colloid template techniques often face significant obstacles such as high cost, complexity, low throughput, and time consumption, limiting their commercialization for practical applications. Recently, the Breath Figure method (BF) has been employed to fabricate polymer films with regular concave surface patterns, which are then utilized to prepare convex-patterned elastomer replica through micromolding (*m* -molding) methods[20]. However, honeycomb film prepared by BF often requires expensive amphiphilic polymers, very humid conditions, and interior strength for multiple molding processes.

Cite this article : Bui V, Le T H, Hoang G H N, Luu A T, Pham T K, Khai T V, La T T H. **Easy and efficient patterning of elastomer dielectric toward commercialization of triboelectric nanogenerator**. *Sci. Tech. Dev. J. – Engineering and Technology* 2024; 7(3):2402-2414.

History
- Received: 02-4-2024
- Revised: 25-5-2024
- Accepted: 22-10-2024
- Published Online: 31-12-2024

DOI :
https://doi.org/10.32508/stdjet.v7i3.1359

To address these challenges, we propose an innovative strategy for creating ordered regular microwell-pattern array on the surfaces of disposed plastic plates such as Petri dishes made from polystyrene, and CD discs made from polycarbonate, which are then exploited as robust molds for preparing convex-microbead-patterned elastomer replicas. The microwell array, being part of the plate, enhances the structural integrity of the mold for repeating the molding process. The patterned PDMS is employed to fabricate TENG device. The electrical output of patterned TENG is characterized and compared to the TENGs using unstructured PDMS. The use of plastic waste as starting materials and the employment of a solution process, without any strict preparation conditions required, enable this approach for massive and cost-effective production.

EXPERIMENTAL METHODS

Materials

Petri dishes and CD discs were sourced from waste disposal sites, thoroughly washed with water to remove dirt, debris, and oil residues, and then air-dried in ambient conditions before storage. Polydimethylsiloxane (PDMS) and curing agent (Sylgard 184) were obtained from Dow Corning (USA). Anhydrous chloroform (99.8%) with amylenes as stabilizers and anhydrous methanol (99.8%) were acquired from Sigma-Aldrich (USA) and used as supplied.

Fabrication of the mw-molds and mb-PDMS replicas

The *mw*-plate molds were prepared by the Improved Phase Separation (IPS) method[21]. The chloroform-methanol mixture, with a ratio of 90:10 (v/v), was prepared by thorough agitation of the two liquids. Following this, polymer plates (Petri dish or CD disc) were immersed in the solvent mixture using a dip-coater, and subsequently withdrawn from the solvent. The samples were then air-dried under normal conditions (~30°C and 65% RH). Dip-coating parameters were fixed to a dipping speed of 30 cm.min^{-1}, withdrawal speed of 50 cm.min^{-1}, and a retention time of 15 s. Upon complete drying, *mw*-plate molds were obtained, and the features of the microwell array could be adjusted by varying the chloroform-methanol ratio. These *mw*-plate molds were then utilized to fabricate the *mb*-PDMS replicas through a micromolding method. The base PDMS and its cross-linker were mixed at a ratio of 10:1 (w/w), poured onto the *mw*-plate molds, and thoroughly degassed before curing at 70 °C for 4 hours. Subsequently, the *mb*-PDMS replicas were obtained by peeling them off from the mold.

Fabrication of microbead-patterned TENG (mb-TENG)

The contact-separation mode TENG was assembled using *mb*-PDMS and aluminum as two tribosurfaces, each with dimensions of 2×2 cm^2, and maintaining a fixed distance of 5 mm between them. Two polylactic acid (PLA) plates, coated with aluminum adhesive on their inner surfaces, were employed as the top and bottom mechanical support substrates for the TENG. The smooth surface of the *mb*-PDMS was adhered to the aluminum, while its patterned side served as the friction surface. Aluminum on the bottom substrate functioned both as the friction surface and the electrode. Electrical wires were connected to the electrodes for electrical output characterization.

Fabrication of gapless triboelectric nanogenerator (gl-TENG)

The *gl*-TENG was assembled utilizing the *mb*-PDMS hybrid and copper mesh (Cu-mesh) as negatively and positively charged surfaces, respectively. Both the electrets with the same size of 3×5 cm^2 were placed in close to one another and sealed along the edges with adhesive tape. Electrical wires were connected to the copper mesh electrode, establishing a single-electrode, gapless TENG.

Characterization methods

The surface morphology of the samples was characterized by using scanning electron microscopy (SEM, JSM-IT2000 InTouchScope, JEOL Ltd.), and optical microscope (XYX-M3230 upright metallurgical microscope, China). The simulation results were achieved using COMSOL Multiphysics software with the assumed surface charge density across electrodes of 0.3425 mC m^{-2}. A freely available software (ImageJ) was utilized to analyze the features of pattern array. The static water contact angle (WCA) was measured utilizing a drop shape analyzer (Phonenix 300, S.E.O, Korea). A pushing tester was applied to generate vertical impulse vibrations to the TENG. Electrical output measurements were conducted using a digital oscilloscope (Model No. SDS1102CML, Siglent, China) and a low-noise current preamplifier (Model No. SR570, Stanford Research Systems, Inc., USA). Additionally, the thickness of the samples was measured by a Elcometer A456CFBS with the T456CF1S probe.

The average power density (P_{av}) was calculated using the following equations.

$$P_{av} = \frac{U_{rms}^2}{R} = \frac{\sqrt{\frac{1}{n}\Sigma U_i^2}}{R}$$

RESULTS AND DISCUSSION

Fabrication of convex and concave patterned PDMS

Figure 1 illustrates the overall fabrication process of convex-patterned elastomers and presents the proposed mechanism for forming a microwell array onto polymer plates by using the IPS method. In Figure 1a, the fabrication begins with the large-scale preparation of a microwell-patterned plate through a one-step dip-coating process. Subsequently, this microwell plate serves as a reusable mold (*mw*-plate mold) for preparing the convex-microbead-patterned elastomer (*mb*-PDMS) via the m-molding method, with experimental details provided in the Experimental Section. Regarding the proposed mechanism for forming a microwell structure on polymeric plates such as Petri dish, it is essential to highlight the crucial roles of the rational mixture solvent composed of chloroform and methanol. Firstly, the solvent dissolves the polymer, leading to formation of a polymer solution adhering to the plate surface (Figure 1b). Secondly, it induces phase separation through solvent evaporation, causing the formation of nonsovent phase, which acts as templating droplets for creating cavities on the plate surface. Thirdly, it promotes the regularity and ordering of microwell array through protecting templating droplets from coalescence (Figure 1c). Notably, the higher evaporation rate of chloroform compared to methanol results in increased methanol content causing phase separation to form a nonsolvent-rich phase. In addition, solvent evaporation significantly reduces the solution surface temperature, potentially facilitating water absorption into the nonsolvent phase, thereby accelerating the growth of the nonsolvent droplets due to methanol's strong hydrophilicity. The influence of methanol content on solubility of polymer in the mixture can be clarified by determining the interaction parameter between polymer and the mixture solvent (See Tables 1 and 2 in Supporting Information.). At low methanol content, the mixture can easily dissolve polymer, as evidenced by small interaction parameters. However, with increasing methanol content (>20%), the solubility of the polymer in the mixture decreases, evidenced by enhanced interaction parameters, leading to the transformation of polymer molecule shape from extended conformation to collapsed globules, resembling nanoparticle-like polymer structures. The accumulation of methanol into the nonsolvent phase facilitates the aggregation of polymer nanoparticles, inducing a gel-like protective layer, which enhances the regularity and ordering of the pattern array. In contrast, the absence of nonsolvent in the BFs solution prevents the formation of the gel-like protective layer, consequently reducing the regularity of patterns prepared with nonpolar linear polymers.

The effect of the nonsolvent phase conformation on the cavity structure is attributed to the spreading coefficient S_p, defined as follows[22]:

$$S_p = \gamma_s - (\gamma_n + \gamma_{sn}),$$

where γ_s, γ_n are the surface tensions of the solution and the nonsolvent, respectively, while γ_{sn} is the interfacial tension between the solution and the nonsolvent phase. To obtain the microwell structure, the nonsolvent phase must be in form of droplet, corresponding to negative S_p. If S_p is positive, the nonsolvent phase is not able to remain droplet form or dissolves into the polymer solution. Therefore, introducing methanol featuring low surface tension results in reduction of γ_n and γ_{sn}, consequently increasing S_p, which is more favorable for forming microwell structures rather than spherical pore structure (See Table 3 in Supporting Information.). Figure 1d demonstrates the method's capability for industrial enlargement of the *mw*-plate mold. As depicted, a Petri dish with uniform pattern arrays can be obtained via a simple dip-coating process in normal air, without the requirement for high humidity conditions. Additionally, by employing this microwell plate as a mold, large-scale *mb*-PDMS replicas were produced, exhibiting excellent flexibility and stretchability, as shown in Figure 1e.

Figure 2 presents the surface and cross-sectional morphologies of microwell-patterned surfaces of both Petri dish and CD disc, alongside the convex-patterned PDMS replica. Optical microscopy images (Figure 2a and Figure 2d) illustrate the formation of uniform pore arrays across the large area of both the Petri dish and CD disc. To gain further insight into the structures, top-view and cross-sectional SEM images of the patterned plates were acquired, as depicted in Figure 2b, 2c, 2e, and 2f. The pores on the Petri dish and CD disc exhibit cylindrical shapes, with the Petri dish having a pore size of 7.2 μm and a pore depth of 6.8 μm, while the CD disc features a pore size of 6.5 μm and a pore depth of 6.0 μm. Subsequently, convex-patterned PDMS electrets were fabricated using the corresponding *mw*-mold through the μ-molding method, such as the *mw*-Petri mold, as shown in Figure 2e, 2f, and 2k. Figure 2e illustrates a large-area uniform convex-microbead array observed on the surface of PDMS. The beads exhibit a diameter of 6.0 μm and a height of 4.6 μm, which values

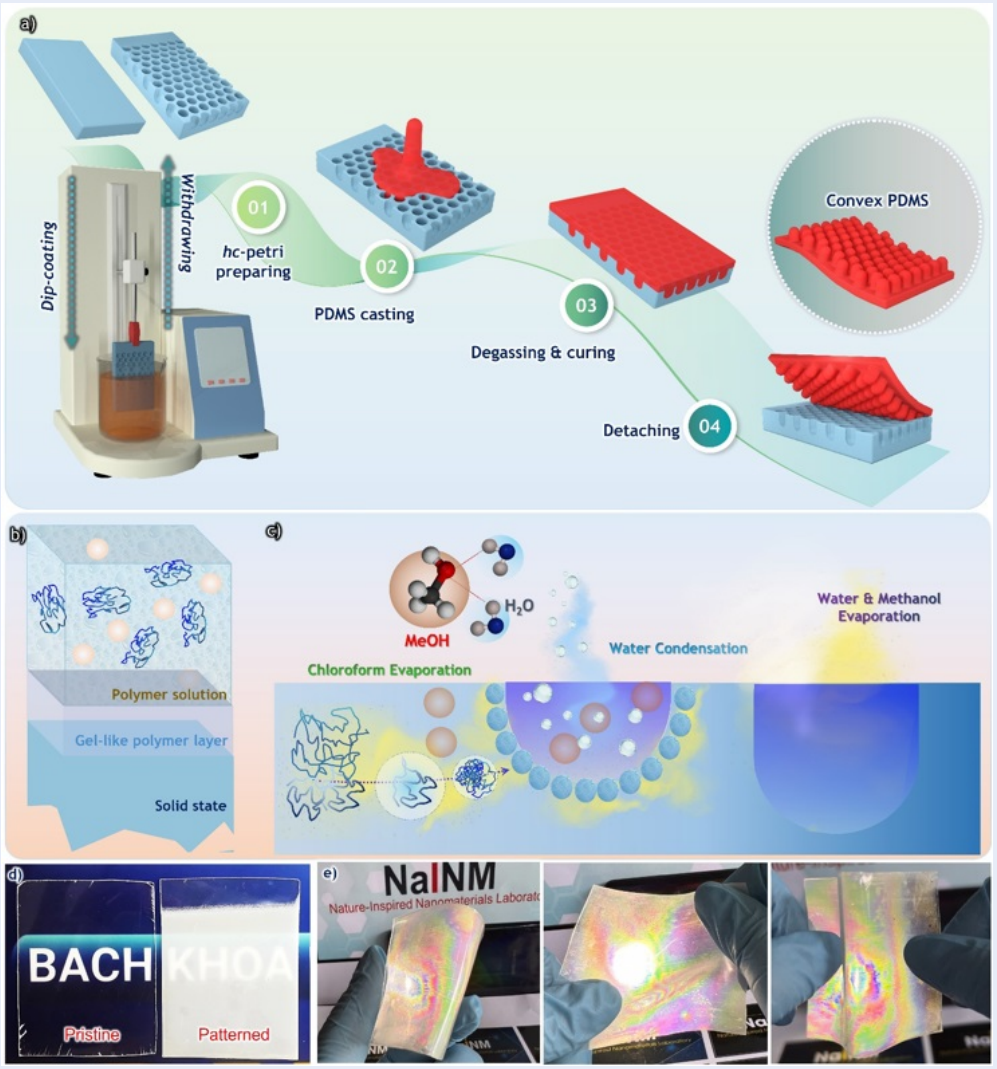

Figure 1: Large-scale fabrication of convex-patterned elastomer electret. (a) Scheme representing the creation of microbeads array onto PDMS elastomer, with the inset showing the practical dip-coating process. (b, c) Schematic illustrating layered structure formation and microwell array formation mechanism on the polymeric plate via the IPS method. (d) Picture of the *mw*-plate mold prepared from Petri dish. (e) Optical pictures of *mb*-PDMS replicas showing flexibility and stretchability.

are smaller than that of the pore size of the *mw*-Petri mold. This reduction in pattern size can be attributed to the shrinkage of PDMS after cross-linking and incomplete filling of the PDMS liquid into the mold cavity.

Application of the patterned PDMS for a TENG

The specific surface area of tribo-materials plays a pivotal role in influencing the contact area available for inducing triboelectrification. COMSOL simulations have demonstrated that the TENG device incorporating a PDMS microbead-pattern array yielded an electrical potential distribution of approximately 400 V, which is about four times higher than that achieved using flat PDMS surfaces (Figure 3a). This notable enhancement can be attributed to the larger specific surface area of the microbead-patterned PDMS. Additionally, frictional interaction between the microbeads and planar surface induced by the deformation of microbeads substantially enhances electrification effectiveness, aligning with findings from prior studies (Figure 3b)[23].

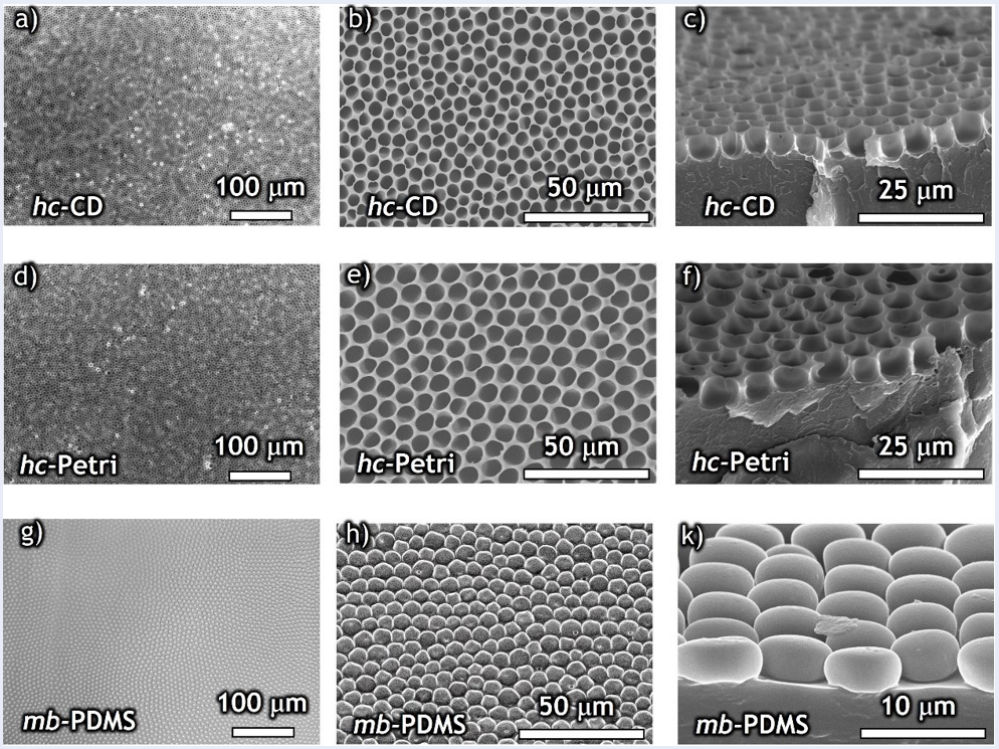

Figure 2: Surface morphologies of the honeycomb-concave molds prepared from disposed CD disc and Petri culture dish, and the microbeads patterned PDMS electret. (a-c), (d-f), (g-h) Optical microscopy, surface SEM and cross-sectional SEM images of honeycomb CD disc, Petri dish, and convex-PDMS, respectively.

The operational mechanism of the *mb*-TENG is elucidated in detail in Figure 3c, illustrating a single contact-separation cycle. Initially, both the *mb*-PDMS and Al surfaces remain uncharged. Upon physical contact between the two surfaces, positive charges accumulate on the Al surface, while corresponding negative charges form on the *mb*-PDMS surface due to contact electrification principle of triboelectric series. With successive contact-separation cycles, the triboelectric charge density on the dielectric surface gradually increases until saturation, with the negative charges effectively retained on the PDMS surface owing to its insulating nature. As the surfaces separate, the electrostatic field arising from the charges induces electron flow from the bottom electrode through the external load to the top electrode until electrostatic equilibrium is reached. Upon the surfaces approaching each other again, the electrostatic field induces electron flow to return from the top electrode to the bottom electrode, restoring the system to the fully pressed equilibrium state before starting new cycles. This process demonstrate single-cycle operation with the voltage signals generated is presented in the inset of Figure 3c.

The COMSOL simulation was conducted to investigate how the structural features of microbead arrays influence the surface potential distribution across TENG devices. The diameter of the microbeads was consistently fixed at 6 μm, while the separations between microbeads were set at 2 μm, 1 μm, 0 μm for *mb*-PDMS1, *mb*-PDMS2, and *mb*-PDMS3, respectively. As illustrated in Figure 4d, 4e, and 4f, a significant decrease in surface potential across the TENG devices corresponds to the reduction in separation. Notably, *mb*-PDMS1, with the largest separation of 1 μm, exhibits the highest surface potential, reaching approximately 600 V. Conversely, for *mb*-PDMS2 and *mb*-PDMS3, as the distance between microbeads decreases to 0.5 μm and 0 μm, respectively, the surface potential variance diminishes to approximately 450 V and 200 V. These simulation results suggest that increasing the separation between microbeads facilitates greater deformation during the contact process with the aluminum foil, thereby enhancing frictional effectiveness.

TENG devices composed of *mb*-PDMS1, *mb*-PDMS2, and *mb*-PDMS3 were fabricated and characterized, and these electrical outputs were compared with a

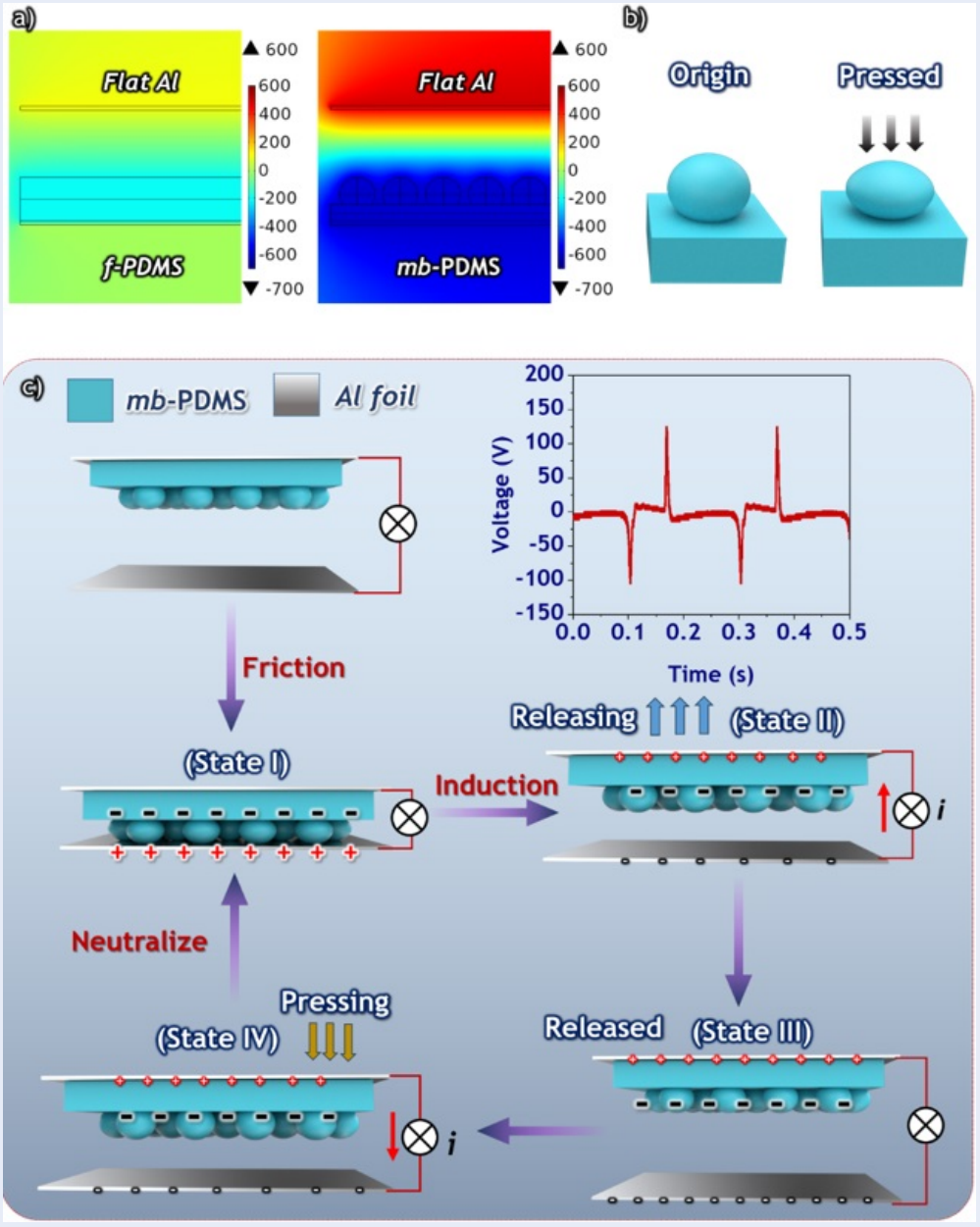

Figure 3: Structural design and working mechanism of the *mw*-TENG. (a) Schematic of triboelectric electric energy generation for one contact−separation cycle of the *mw*-TENG. (b) Current signals obtained during 1 cycle contact–separation of TENGs using flat and microbead-patterned PDMS. (c) The electrical potential distribution of flat and microbead-patterned PDMS simulated via COMSOL Multiphysics software.

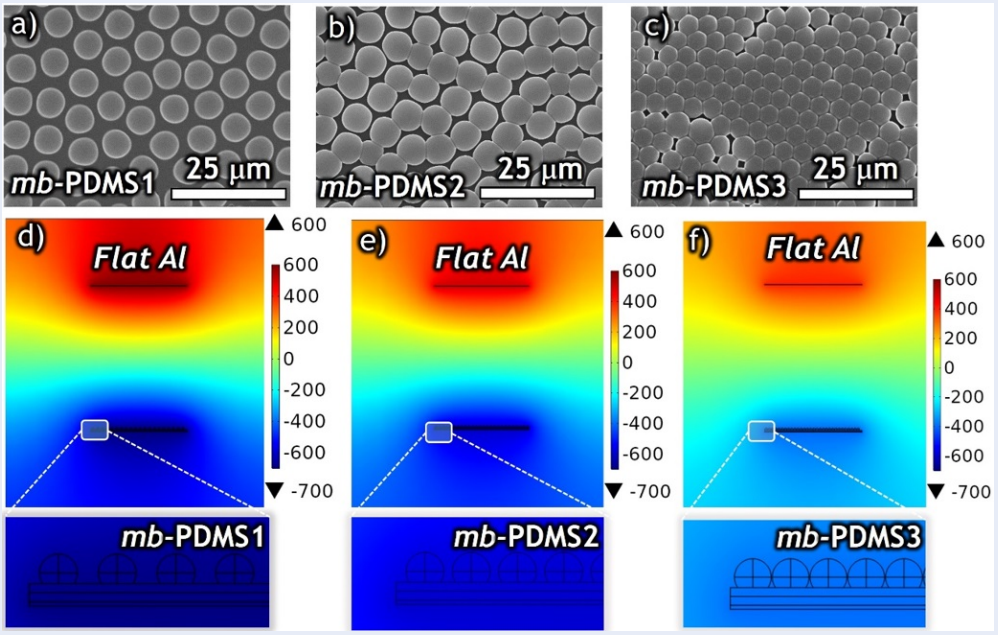

Figure 4: The influence of pattern features on surface potential distribution of the *mb*-TENG. (a-c) Surface morphologies of *mb*-PDMS electrets with various pattern features. (d) The COMSOL Multiphysics simulation results for electrical potential distribution of the *mb*-PDMS with different pattern features.

TENG using normal flat PDMS (*f*-TENG) as a reference. The V_{OC} and I_{SC} of the *mb*-TENGs and *f*-TENG are as shown in Figure 5a and 5b. Both the V_{OC} and I_{SC} of the *mb*-TENGs were significantly enhanced compared to the *f*-TENG. Among these *mb*-TENGs, the TENG using the *mb*-PDMS1 exhibited the highest electrical output performance, yielding a V_{OC} of 185 V and a I_{SC} of 20.5 μA. The enhancement of electrical ouput can be attributed to enlarged friction area, optimal contact force and effective stress of the patterned surface compared to the planar surface, thereby enhancing the triboelectric effect[24]. The dependence of V_{OC} and I_{SC} corresponding to external resistances was investigated to determine the power generation effectiveness of the *mb*-TENG, as shown in Figure 4c. Due to ohmic loss effect, V_{OC} increased while I_{SC} decreased with an increase of the external loads. Additionally, the average power densities of the *mb*-TENG and *f*-TENG were characterized, as depicted in Figure 5. The output power of the *mb*-TENG and *f*-TENG could reach maximum values of 3.92 W.m^{-2} at matched loads of 10 MΩ and 0.75 W.m^{-2} at matched loads of 20 MΩ, respectively. The results indicate that the power generation efficiency of the *mb*-TENG is over 5 times higher than that of the *f*-TENG. Figure 6 demonstrates the high power output of the *mb*-TENG devices. The *mb*-TENG device offers ability to instant activation of a text panel with over 200 green LEDs even with a small vibration force, as depicted in Figure 6a. Furthermore, the *mb*-TENG effectively charged commercial capacitors through a rectifier bridge. Figure 6b displays the charging rate curves of capacitors charged using the *mb*-TENG devices with a size of 2×2 cm^2 at a frequency of 5 Hz. The results indicated that small-capacity capacitors (2.2 μF) could be rapidly charged to over 3 V, while larger capacitors (10 μF) reached a voltage of nearly 3 V within a short duration of 50 s. Furthermore, the stability of the electrical output generated by the *mb*-TENG device was validated through the charging and discharging curves of a low-power microelectronic device, as shown in Figure 6c. Additionally, as depicted in Figure 6d, a 10 μF capacitor was utilized as a storage component to power a wristwatch after a charging process facilitated by the *mb*-TENG. The charging curve of the capacitor (Figure 6e) indicated that it was charged to over 4 V within 150 s, enabling it to successfully power a wristwatch under normal working conditions for at least 20 s. These results highlight the high potential of the *mb*-TENG devices for powering low-power wearable electronic devices.

PDMS is widely recognized as a biomaterial for various biomedical applications owing to its biocompatibility, flexibility, and inertness, making it suitable

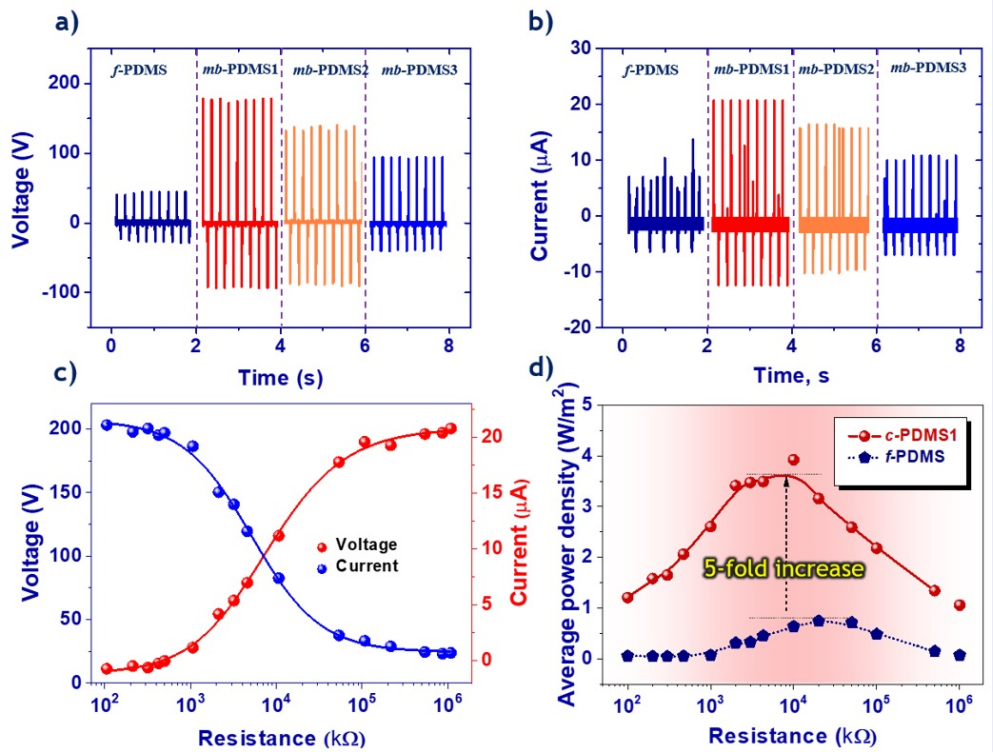

Figure 5: Characterization of electrical output of the *mb*-TENG. (a, b) Open-circuit voltages (V_{OC}) and short-circuit current (I_{SC}) of TENGs using flat and various structured PDMS electrets. (c) Dependence of V_{OC} and current of I_{SC} TENG using the *mb*-PDMS1 on the resistance of external loads, respectively. (d) Change of the average power density of TENGs made from *f*-PDMS and *mb*-PDMS1 on the resistance of loads, respectively.

for integration into wearable human health-related devices. Figure 7a illustrates the three-dimensional structural design of the single electrode *gl*-TENG, composed of the *mb*-PDMS as a negative charged surface and copper mesh as a counter electrode. The convex microbead patterns on PDMS surface and the concave structure of copper mesh naturally create a gap in the *gl*-TENG without the need for an external spacer. This device exhibits superior flexibility, biocompatibility, and ease of attachment to the human body, as demonstrated in Figure 7b. The simulated results via COMSOL of the corresponding bending states validate working principle of the *gl*-TENG, as shown in Figure 7c.

In the era of IoHT, healthcare sensors play a pivotal role and are increasingly popular for self-health equipment. To broaden practical applications of self-health monitoring, improvements in electrical output, biocompatibility, and integrability are essential. The *gl*-TENG operating in single-electrode mode is strategically designed to function both as an body motion energy harvester and a self-health monitoring sensor. Figure 8 llustrates the utilization of the *gl*-TENG as a self-powered sensor for monitoring body motion. Positioned at various body parts such as the elbow, knee, and foot, the *gl*-TENG sensors generate electrical signals under different body movement conditions, including walking, jogging, and running. Oscillatory motions induce periodic contact-separation cycles, leading to the generation of periodic electrical signals. Moreover, the amplitude of the output signals increases with higher bending angles. As illustrated in Figure 8a, with elbow flexion ranging from 30 to 90°, the V_{OC} increases from approximately 25 V to 90 V. Similarly, when attached to knee, under normal walking conditions, the V_{OC} reaches approximately 100 V, and during jogging or running, an increase in the knee bending angle raises the V_{OC} from 150 to 200 V due to the augmented contact area between the TENG and joints, as shown in Figure 8b. When attached to the sole, the device during walking or jogging establishes extensive contact with the ground, resulting in a V_{OC} of approximately 300 V. Furthermore, running generates an even higher voltage output, peaking at 400 V, due to amplified force and enlarged contact area, as shown in Figure 8c. This application demonstrates

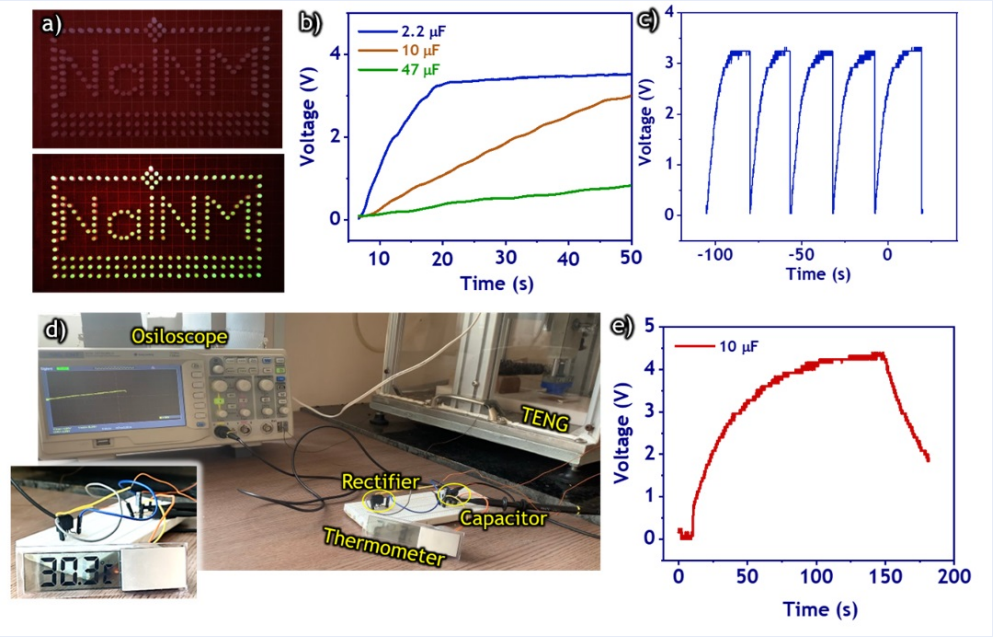

Figure 6: Demonstration of the *mb*-TENG as a mechanical energy harvester for powering microelectronics. (a) Instant activation of 200 green LEDs. (b) Charging capacitors with various capacitances. (c) Multiple cycles of charging and discharging curves of a 2.2 μF capacitor. (d) Illustration of charging capacitor and powering an electronic temperature sensor. (e) Charging and discharging curves of 47 mF-capacitor and powering for the temperature sensor.

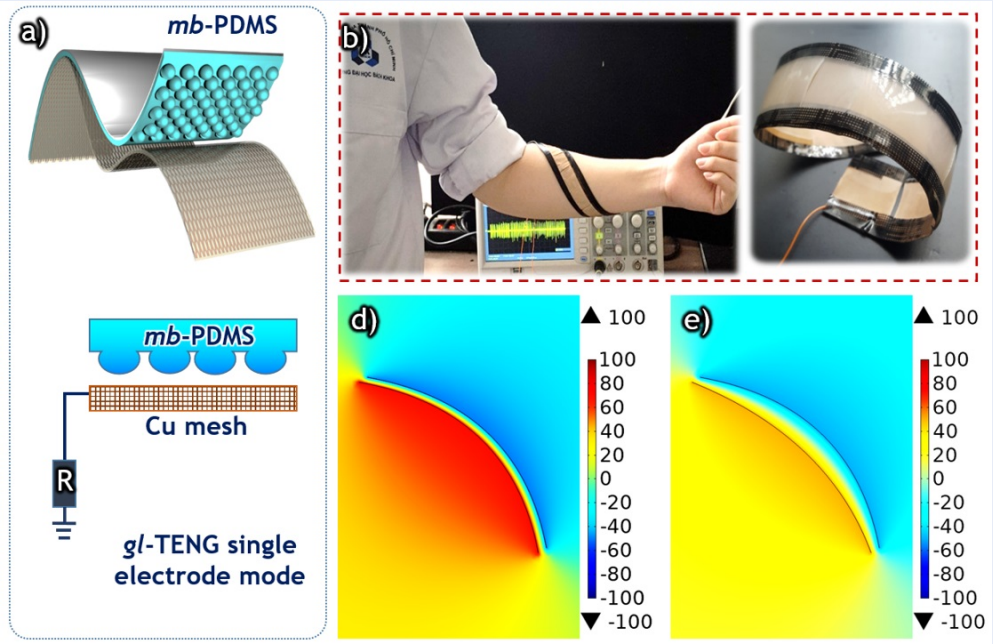

Figure 7: Fabrication and working principle of the breathable wearable *gl*-TENG. (a) Structural design of the *gl*-TENG. (b) Demonstration of the *gl*-TENG ulilization for harvesting mechanical energy from arm shaking. (c, d) COMSOL simulated results of the *gl*-TENG.

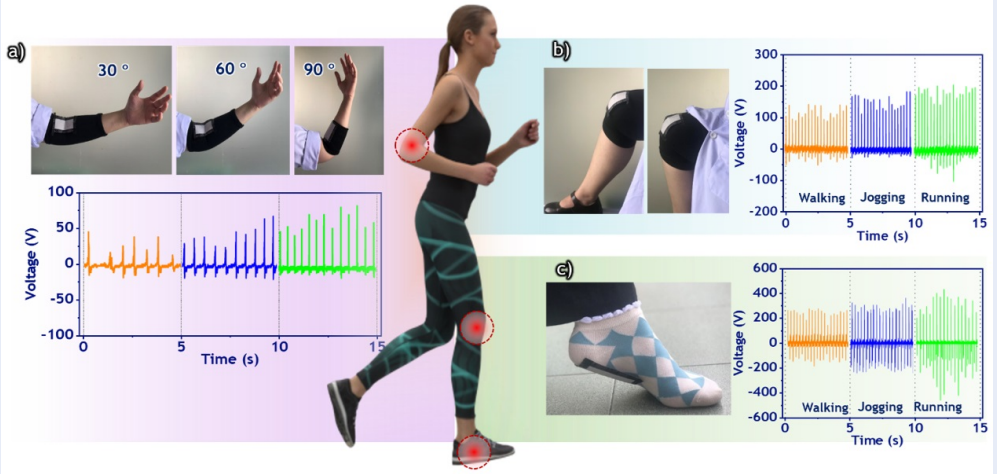

Figure 8: Electrical signals from the *gl*-TENG sensor attached to the elbow, knee and foot during walking, jogging, and running.

the superiority of the *gl*-TENG as a self-powered sensor in IoHT applications.

CONCLUSION

In this study, we have successfully developed a robust microwell plate mold (*mw*-plate mold) using recycled plastic materials such as Petri dishes and CD discs through a scalable one-step dip-coating process. This mold was then utilized to fabricate microbead-patterned PDMS (*mb*-PDMS) replicas via micromolding techniques. Our findings demonstrate that the *mw*-plate mold exhibits exceptional structural integrity, enabling multiple molding processes due to its reinforced design. The *mb*-TENG device, constructed with the *mb*-PDMS and aluminum tribosurfaces, exhibits a remarkable average power density of 3.92 $mW \times m^{-2}$, corresponding to an V_{OC} of 185V and a I_{SC} of 20 μA. This represents a significant 5-folds power enhancement compared to TENG using flat PDMS. Additionally, it serves as a self-powered multifunctional wearable sensor for physiological monitoring based on triboelectric principles. We believe that the cost-effectiveness, scalability, and efficiency of surface patterning demonstrated in our approach, utilizing recycled plastic wastes, could pave the way for the commercialization of future TENG technologies, particularly for blue energy harvesting applications requiring large-scale deployment of TENG devices.

SUPPORTING INFORMATION

Supporting information file (PDF)

CONFLICT OF INTEREST

The authors declare that they have no known competing financial interests or personal relationships that could have appeared to influence the work reported in this paper.

AUTHORS' CONTRIBUTIONS

Van-Tien Bui: Conceptualization, Resources, Writing –Reviewing and Editing; Thu Ha Le: Methodology, Investigation, Formal analysis, Data curation; Gia Huy Nguyen Hoang: Investigation, Formal analysis, Data curation; Tuan Anh Luu: Discussion, software; Trung Kien Pham: Discussion; Van Khai Tran: Writing –Reviewing and Editing; Thi Thai Ha La: Funding acquisition.

ACKNOWLEDGMENT

This research is funded by Vietnam National University HoChiMinh City (VNU-HCM) under grant number 562-2022-20-03. We acknowledge Ho Chi Minh City University of Technology (HCMUT), VNU-HCM for supporting this study.

SUPPORTING INFORMATION

Tables 1, 2 and 3

The interaction parameter (χ) between the solvent and the polymer can be determined from the difference of their Hasen solubility parameters (HSP) using the following expression:

$$\chi = \frac{V_m}{RT}[(\delta_{d1} - \delta_{d2})^2 + (\delta_{p1} - \delta_{p2})^2 + (\delta_{h1} - \delta_{h2})^2]$$

Table 1: The interaction parameter between polymer and the mixture solvent

	dD	dH	d	M	Density
	22.8	4.3	5.8		
ChL	17.8	5.7	3.1	80.5	1.49
MeOH	15.1	12.3	22.3	40.6	0.792

Table 2: The interaction parameter between polymer and the mixture solvent

MeOH content (%)	Interaction parameter
0	0.85906
5	0.76851
10	0.76176
15	0.83882
20	0.99969
30	1.57284
40	2.48122
50	3.72482
60	5.30365
70	7.2177
80	9.46698
90	12.05149
100	14.97121

where $\delta_d, \delta_p, \delta_h$ values represent the HSPs of the dispersion force, dipolar intermolecular force, and hydrogen bond between two molecules, respectively. R denotes the ideal gas constant (8.314 J $mol^{-1}K$) and T is the environment temperature (298 K^{-1}). V_m is defined as the molar volume of the repeating unit of the polymer.

$$V_m = \frac{M}{\rho}$$

where M represents the molar mass of the structural unit and ρ denotes the density of polymer. For the solvent mixtures, the solubility parameter d is related to the volume fraction φi and the solubility parameter φi of each component using the following expression:

$$\delta = \Sigma \varphi_i \delta_i$$

REFERENCES

1. Mao J, et al. A health monitoring system based on flexible triboelectric sensors for intelligence medical internet of things and its applications in virtual reality. Nano Energy. 2023;118:108984;.
2. Karimzadehkhouei M, Ali B, Jedari Ghourichaei M, Alaca BE. Silicon Nanowires Driving Miniaturization of Microelectromechanical Systems Physical Sensors: A Review. Adv Eng Mater. 2023;25(12):2300007;.
3. Qu Z, et al. A Triboelectric Nanogenerator Based on Pendulum-Rotation Transmission Mechanism for Harvesting Continuous Low-Frequency Mechanical Energy. Adv Mater Technol;.
4. Chu H, Xue J, Luo D, Zheng H, Li Z. Advances in Wearable Multifunctional Devices Based on Human-Body Energy Harvesting. Adv Mater Technol;.
5. Zhao Z, Hu Y. Textile Triboelectric Nanogenerator: Future Smart Wearable Energy-Integration Technology. Adv Mater Technol;.
6. Zou Y, et al. A Flexible, Adaptive, and Self-Powered Triboelectric Vibration Sensor with Conductive Sponge-Silicone for Machinery Condition Monitoring. Small;.
7. Huang J, et al. A Wind Bell Inspired Triboelectric Nanogenerator for Extremely Low-Speed and Omnidirectional Wind Energy Harvesting. Small Methods;.
8. Liu D, et al. A Dual-Mode Triboelectric Nanogenerator for Efficiently Harvesting Droplet Energy. Small;.
9. Ying Q, Wu J, Liu C. Multi-Track Triboelectric Nanogenerator Toward Omnidirectional Ocean Wave Energy Harvesting. Adv Mater Technol. 2024;9(5):2301824;.
10. Li Y, et al. Advanced Dielectric Materials for Triboelectric Nanogenerators: Principles, Methods and Applications. Adv Mater;.
11. Pang Y, He T, Liu S, Zhu X, Lee C. Triboelectric Nanogenerator-Enabled Digital Twins in Civil Engineering Infrastructure 4.0: A Comprehensive Review. Adv Sci;.
12. Lee G, et al. Anisotropic Fluorinated-Elastomer-Blended Micro-Dominoes for Wearable Triboelectric Nanogenerators. Adv Funct Mater;.
13. Wang J, et al. Contact Electrification Induced Multicolor Self-Recoverable Mechanoluminescent Elastomer for Wearable Smart Light-Emitting Devices. Adv Opt Mater. 2023;11(12):2203112;.
14. Karagiorgis X, Khandelwal G, Beniwal A, Chirila R, Skabara PJ, Dahiya R. Polydimethylsiloxane Foam-Based Fully 3D Printed Soft Pressure Sensors. Adv Intell Syst;.
15. Nam Y, et al. Ultra-Thin GaAs Single-Junction Solar Cells for Self-Powered Skin-Compatible Electrocardiogram Sensors. Small Methods;.
16. Kim S, Yoo D, Lim J, Kim J. Simple and Effective Patterning Method of Liquid-Metal-Infused Sponge Electrode for Fabricating 3D Stretchable Electronics. Adv Mater Technol;.
17. Silicone Elastomers-Based Miniature Soft Robots. In: Untethered Miniature Soft Robots. John Wiley & Sons, Ltd; 2024. p. 25-72;.
18. He C, et al. Irreversible Bonding of Polydimethylsiloxane-Lithium Niobate using Oxygen Plasma Modification for Surface Acoustic Wave based Microfluidic Application: Theory and Experiment. Small Methods;.
19. An Y, et al. Efficient preparation of polydimethylsiloxane-based phase change composites with sandwich structure. Polym Compos;.
20. Gong J, Xu B, Tao X. Breath Figure Micromolding Approach for Regulating the Microstructures of Polymeric Films for Triboelectric Nanogenerators. ACS Appl Mater Interfaces. 2017;9(5):4988-4997;.

Table 3: Surface tensions of liquids at 25 °C.

Liquids	Surface tension ($mN.m^{-1}$)	Interfacial tension with water ($mN.m^{-1}$)
Water	72.8	0
Chloroform	26.5	33.5
Tetrahydrofuran	26.4	
Methanol	27.5	0

21. Bui V-T, Thuy LT, Choi JS, Choi HS. Ordered cylindrical micropatterned Petri dishes used as scaffolds for cell growth. J Colloid Interface Sci. 2018;513:161-169;.
22. Ding J, Zhang A, Bai H, Li L, Li J, Ma Z. Breath figure in non-aqueous vapor. Soft Matter. 2013;9(2):506-514;.
23. Bui V-T, et al. Treefrog Toe Pad-Inspired Micropatterning for High-Power Triboelectric Nanogenerator. Adv Funct Mater. 2019;29(28):1901638;.
24. Bui V-T, et al. High-temperature operatable triboelectric nanogenerator using microdome-patterned polyimide for self-powered sensors. Nano Energy. 2022;101:107612;.

Tạp chí Phát triển Khoa học và Công nghệ – Engineering and Technology 2024, 7(3):2402-2414

Open Access Full Text Article

Bài nghiên cứu

Phương pháp tạo hình đơn giản cho vật liệu điện môi đàn hồi ứng dụng trong thiết bị phát điện nano ma sát TENG

Bùi Văn Tiến[1,2], Lê Thu Hà[1,2], Nguyễn Hoàng Gia Huy[1,2], Lưu Tuấn Anh[1,2], Phạm Trung Kiên[1,2], Trần Văn Khải[1,2,*], La Thị Thái Hà[1,2,*]

TÓM TẮT

Thiết bị phát điện nano ma sát (TENG) là một công nghệ tiên tiến trong khai thác năng lượng xanh, đóng vai trò quan trọng như một nguồn cung cấp điện cho các thiết bị điện tử di động tự cấp nguồn. Tuy nhiên, việc đạt được hiệu suất điện cao với chi phí thấp và khả năng sản xuất quy mô lớn vẫn là một thách thức lớn đối với ứng dụng thực tiễn và thương mại hóa TENG. Trong nghiên cứu này, chúng tôi đề xuất một phương pháp tạo hình bề mặt vật liệu điện môi đàn hồi mang tính đột phá, có khả năng mở rộng và chi phí thấp nhằm nâng cao tiềm năng thương mại của TENG. Phương pháp này sử dụng khuôn nhựa có bề mặt vi cấu trúc tổ ong (*mw*-plate mold), được chế tạo từ nhựa phế thải như đĩa Petri và đĩa CD thông qua quy trình nhúng phủ một bước. Khuôn này sau đó được sử dụng để tạo bản sao polydimethylsiloxane với vi cấu trúc hạt lồi (*mb*-PDMS) bằng kỹ thuật đúc khuôn vi mô. Kết quả cho thấy khuôn tổ ong duy trì độ bền cấu trúc vượt trội qua nhiều chu kỳ đúc nhờ khả năng gia cường của nền nhựa. Hơn nữa, thiết bị TENG sử dụng *mb*-PDMS đạt mật độ công suất trung bình 3,92 $mW{\cdot}m^{-2}$, với điện áp hở mạch (V_{OC}) 185 V và dòng ngắn mạch (I_{SC}) 20 μA, cao hơn 5 lần so với TENG không có cấu trúc bề mặt, chứng minh hiệu quả điện hóa được cải thiện đáng kể thông qua kỹ thuật tạo hình bề mặt. Chúng tôi tin rằng phương pháp tạo hình bề mặt vật liệu điện môi đàn hồi có chi phí thấp, khả năng sản xuất quy mô lớn và hiệu suất cao có thể mở ra triển vọng mới trong thương mại hóa TENG, đặc biệt là trong khai thác năng lượng đại dương, nơi yêu cầu triển khai mạng lưới lớn các thiết bị TENG.

Từ khoá: Cấu trúc tổ ong, tạo hình bề mặt, đúc khuôn, vật liệu đàn hồi, thiết bị phát điện nano ma sát

[1]*Khoa Công nghệ Vật Liệu, Trường Đại học Bách Khoa, 268 Lý Thường Kiệt, Quận 10, TP. Hồ Chí Minh, Việt Nam.*

[2]*Đại học Quốc Gia TP. Hồ Chí Minh, Phường Linh Trung, TP. Hồ Chí Minh, Việt Nam*

Liên hệ

Trần Văn Khải, Khoa Công nghệ Vật Liệu, Trường Đại học Bách Khoa, 268 Lý Thường Kiệt, Quận 10, TP. Hồ Chí Minh, Việt Nam.

Đại học Quốc Gia TP. Hồ Chí Minh, Phường Linh Trung, TP. Hồ Chí Minh, Việt Nam

Email: tvkhai1509@hcmut.edu.vn

Liên hệ

La Thị Thái Hà, Khoa Công nghệ Vật Liệu, Trường Đại học Bách Khoa, 268 Lý Thường Kiệt, Quận 10, TP. Hồ Chí Minh, Việt Nam.

Đại học Quốc Gia TP. Hồ Chí Minh, Phường Linh Trung, TP. Hồ Chí Minh, Việt Nam

Email: lathaihapolyme@hcmut.edu.vn

Lịch sử

- Ngày nhận: 02-4-2024
- Ngày sửa đổi: 25-5-2024
- Ngày chấp nhận: 22-10-2024
- Ngày đăng: 31-12-2024

DOI : https://doi.org/10.32508/stdjet.v7i3.1359

Trích dẫn bài báo này: Tiến B V, Hà L T, Huy N H G, Anh L T, Kiên P T, Khải T V, Hà L T T. **Phương pháp tạo hình đơn giản cho vật liệu điện môi đàn hồi ứng dụng trong thiết bị phát điện nano ma sát TENG**. *Sci. Tech. Dev. J. - Eng. Tech.* 2024, 7(3):2402-2414.